Euro. Jnl of Applied Mathematics (2014), *vol.* 25, *pp.* 655–680.
doi:10.1017/S0956792514000217

Unsteady flow over a submerged source with low Froude number

CHRISTOPHER J. LUSTRI[1] and S. JONATHAN CHAPMAN[2]

[1] *School of Mathematics and Statistics, University of Sydney, Sydney, NSW 2006, Australia*
E-mail: christopher.lustri@sydney.edu.au
[2] *Oxford Centre for Industrial and Applied Mathematics, Mathematical Institute, University of Oxford, Oxford OX1 3LB, UK*

(*Received 18 October 2013; revised 4 July 2014; accepted 8 July 2014; first published online 4 August 2014*)

In the low-Froude number limit, free-surface gravity waves caused by flow past a submerged obstacle have amplitude that is exponentially small. Consequently, these cannot be represented using an asymptotic series expansion. Previous studies have considered linearized steady flow past a submerged source in infinite-depth fluids, in which exponential asymptotics were used to determine the behaviour of downstream longitudinal and transverse free-surface gravity waves. Here, unsteady flow past a submerged source in an infinite-depth fluid is investigated, with the free surface taken to be initially waveless. The source is taken to be weak, and the flow is linearized about the undisturbed solution. Exponential asymptotics are applied to determine the wave behaviour on the free surface in terms of the two-dimensional plan-view, in order to show how the free surface waves evolve over time and eventually tend to the steady solution.

Key words: Free-surface potential flows; Gravity waves; Singular perturbations

1 Introduction

1.1 Background

There have been many studies of water waves on unsteady flows, and a detailed historical summary of water wave theory is given by Craik (2004). Important early results include that of Havelock (1949), who examined the behaviour of surface waves caused by flow past a submerged cylinder starting from rest, formulating the wave resistance in terms of an integral equation. This investigation also noted that the formulation derived in Havelock (1917) could be applied to unsteady flows with an obstacle represented as a combination of sources and sinks. John (1953) used a Lagrangian formulation to find steady deep water waves; however, this method (later extended to more general flow configurations by Longuet-Higgins, 1980) could also be applied to unsteady free-surface flows.

More recently, Cole (1985) considered unsteady flow past a small bump, finding an integral expression for the behaviour of the surface for the linearized problem and solving the full non-linear KdV equation numerically. These two regimes were then connected by deriving a quasi-linear theory. Abou-Dina (2001) investigated unsteady gravity waves

over a base topography caused by an initial prescribed free-surface position, using both the linearized theory and computing solutions to the full non-linear formulation. Xue & Yue (1998) computed the unsteady free-surface behaviour for flow due to an impulsively started point sink over a range of Froude numbers. Zhu & Zhang (1997) also computed non-linear flows over a submerged obstacle for a range of Froude numbers. Importantly, this investigation found that for sub-critical flows, a submerged obstacle moving with uniform velocity (equivalent to a stationary obstacle in a uniform flow field) produced a steady wavetrain that spreads over time.

Analytical studies of unsteady gravity waves have been performed in several asymptotic limits. Liu & Tao (2001) formulated an integral expression for the far-field wave behaviour caused by an impulsively-started submerged body, while Lu (2009) determined the far-field unsteady wave behaviour caused by an oscillating Stokeslet. Shen (1969) found an asymptotic expression for unsteady long waves in a three-dimensional shallow channel with arbitrary base topography and small lateral velocity. Ockendon & Wilmott (1986), and Wilmott (1987) used matched asymptotic expansions to determine the behaviour of a free-surface flow past a small spheroid and arbitrary two-dimensional obstruction respectively, both in the case of arbitrary motion.

A number of asymptotic analyses have been performed in the small-time limit, such as the problem of flow due to an impulsively-started submerged cylinder (Tyvand & Miloh, 1995a,b), a line source (Tyvand, 1992) or sink (Stokes *et al*., 2003), and a point sink (Tyvand, 1993). In addition to the small-time limit, Forbes *et al*. (2008) also considered the large-time asymptotic limit for an impulsively-started point sink submerged in a fluid.

None of these investigations, however, considered unsteady waves in the low-Froude number limit, where the Froude number represents the ratio of inertial to gravitational force, defined in (2.4). This limit has been explored in several previous studies, particularly in the context of ship hydrodynamics, using asymptotic power series methods. Ogilvie (1968) considered the problem of a submerged two-dimensional object, noting that the asymptotic series in powers of the Froude number failed to produce wave behaviour on the calculated free surface. Dagan & Tulin (1972) considered the wave resistance of a blunt bow, also obtaining waveless solutions up to second order in the Froude number. Vanden-Broeck *et al*. (1978) investigated several free-surface flow problems in this limit, using Padé approximant representations of the solutions in order to obtain discontinuous free-surface profiles. In more general problems from fluid dynamics, Peregrine (1972) considered the low-Froude number problem of flow due to a line source or sink, finding the solution to be waveless up to fourth order. The wavelessness of the free surface in these expansions is now known as the low-speed paradox.

It is well-known that the free-surface gravity waves present on potential flow over a submerged obstacle are exponentially small in this limit (Ogilvie, 1968), and hence cannot be seen using classical asymptotic power series. However, numerous studies have applied exponential asymptotic techniques in order to determine the behaviour of gravity waves in the low-Froude number limit. These studies considered flow past obstacles in both two (Chapman & Vanden-Broeck, 2006; Trinh & Chapman, 2010; Trinh *et al*., 2011; Lustri *et al*., 2012, 2013) and three dimensions (Lustri & Chapman, 2013). Importantly, each of these studies considered the problem to be steady. For example, in Lustri & Chapman

(2013), the authors determined the behaviour of gravity waves in three dimensions caused by steady, infinite-depth flow over a submerged source.

Here, we consider free-surface gravity waves caused by unsteady, infinite-depth flow over a point source in three dimensions. This is the unsteady version of the steady problem considered by Lustri & Chapman (2013). As in the analysis of the steady problem, we consider the strength of the source to be weak, and linearize the problem in this parameter, fixing the position of the boundary. Additionally, we prescribe a waveless initial state for the flow. We subsequently apply exponential asymptotic techniques directly to the flow equations in order to determine the unsteady surface behaviour, and hence how the waves evolve in time and tend to the steady state behaviour obtained by Lustri & Chapman (2013).

Finally, we note that exponential asymptotic methods have been used to consider steady free-surface fluid flow problems in other limits. Chapman & Vanden-Broeck (2002) applied exponential asymptotic methods to determine the behaviour of upstream capillary waves for flow over a submerged obstacle in the low-Bond number limit, while the more complicated case of gravity-capillary waves on two-dimensional flow with low-Froude number and Bond number has been considered in both linear (Trinh & Chapman, 2013a) and non-linear (Trinh & Chapman, 2013b) regimes. The behaviour of weakly non-local solitary waves was investigated by Grimshaw & Joshi (1995) and Grimshaw (2011), as well as by Trinh (2011) using methods similar to those presented here. Keller & Ward (1996) considered slow flow past a cylinder with small Reynolds number, using exponential asymptotics to determine the drag on the cylinder, and local asymmetry of the flow.

1.2 Methodology

It was Stokes (1864) who first observed that a function containing multiple exponentials in the complex plane can contain curves along which the behaviour of the sub-dominant exponential changes rapidly. These curves are known as *Stokes lines*. This investigation will apply the exponential asymptotic technique developed by Olde Daalhuis *et al.* (1995) and extended by Chapman *et al.* (1998) for investigating the smooth, rapid switching of exponentially small asymptotic contributions across Stokes lines. The methodology is described at length in Lustri & Chapman (2013), and we will therefore simply outline the details here.

The first step in this technique is to express the solution as an asymptotic power series, such as

$$f(x;\epsilon) \sim \sum_{n=0}^{\infty} \epsilon^n a_n(x) \qquad \text{as} \quad \epsilon \to 0.$$

Because we are considering a singular perturbation problem, the series will be divergent. The approximation error can be minimized by truncating the series optimally. Chapman *et al.* (1998) observed that the optimal truncation point tends to become large in the asymptotic limit, and hence the form of the *late-order terms* of the series (that is, the form of a_n in the limit that $n \to \infty$) is sufficient to truncate the asymptotic series optimally.

https://doi.org/10.1017/S0956792514000217 Published online by Cambridge University Press

They propose that the late-order terms are given by a sum of expressions with the form

$$a_n \sim \frac{A\Gamma(n+\gamma)}{\chi^{n+\gamma}} \qquad \text{as} \quad n \to \infty, \tag{1.1}$$

where Γ is the gamma function (see Abramowitz & Stegun 1972), and A, γ and χ are functions that do not depend on n. Each of these factorial-over-power expressions is associated with a particular singularity in the early-order terms, and χ will be zero at the singularity. In the current study, different expressions for χ correspond to different classes of wave behaviour.

Furthermore, they note that the late-order term behaviour given in (1.1) is related to applying a WKB ansatz of the form $A\mathrm{e}^{-\chi/\epsilon}$ to the equation for f linearized about the truncated expansion. Dingle (1973) notes that Stokes switching takes place on curves where the singulant χ is purely real and positive, known as Stokes lines. In the problem considered here, these Stokes lines correspond to curves along which water wave behaviour is switched on or off.

Once the form of the late-order terms is established, we may find the smallest term in the series, and hence truncate the series optimally. This gives

$$f(x;\epsilon) = \sum_{n=0}^{N-1} \epsilon^n a_n(x) + R_N,$$

where $N(x;\epsilon)$ is the optimal truncation point, and R_N is the now exponentially small remainder term, which describes the behaviour of exponentially-small water waves. We now follow the method of Olde Daalhuis *et al.* (1995) and use the resultant expression to determine the switching behaviour of R_N across Stokes lines.

We make one final remark before we proceed to apply these techniques to our free-surface problem. The exponential asymptotic methodology of Olde Daalhuis *et al.* (1995) and Chapman *et al.* (1998) was developed for investigating ordinary differential equations. Because our free surface is two-dimensional, we will require the extension of these techniques to partial differential equations which was developed by Chapman & Mortimer (2005) and used in Lustri & Chapman (2013).

Initially, the method is identical, however in some partial differential equations (and indeed, in higher-order differential equations), further Stokes switching may occur in the remainder itself, such that

$$R_N = \mathrm{e}^{-\chi/\epsilon} \sum_{n=0}^{M-1} \epsilon^n R_N^{(n)} + S_M,$$

where S_M is the new (doubly) exponentially sub-dominant remainder term. The relative size of these exponentials may change depending on where we are on the free surface. This behaviour allows for switching to occur between different classes of exponentially-small wave behaviour.

There is, however, a second variety of switching behaviour that is relevant to the current investigation and was not discussed in Lustri & Chapman (2013), known as the higher-order Stokes phenomenon. This behaviour was observed by Aoki *et al.* (2002), and explained in detail by Howls *et al.* (2004) and Chapman & Mortimer (2005). These studies

https://doi.org/10.1017/S0956792514000217 Published online by Cambridge University Press

noted that higher-order Stokes switching behaviour may be present when there are three or more exponential contributions present in the solution. Higher-order Stokes switching was not present in the steady solution considered in Lustri & Chapman (2013), but it will play a role in the unsteady problem.

When an ordinary Stokes line is crossed, an exponentially small contribution is switched on, the size of which is governed by a Stokes switching parameter. When a higher-order Stokes line is crossed, this switching parameter itself is switched on or off. The effect of this higher-order switching is that ordinary Stokes lines are switched on or off as higher-order Stokes lines are crossed. Higher-order Stokes lines originate at the intersection of multiple Stokes lines in the complex plane, known as Stokes crossing points.

Howls *et al.* (2004) showed that when a problem contains three or more singulant contributions, associated with χ_1, χ_2 and χ_3, the higher-order Stokes lines must follow curves satisfying the criterion

$$\mathrm{Im}\left[\frac{\chi_3-\chi_2}{\chi_3-\chi_1}\right]=0.$$

Unlike the steady problem (Lustri & Chapman, 2013), unsteady free-surface flow does contain three interacting exponentially-small asymptotic contributions, and hence higher-order Stokes lines play a role in the solution. Consequently, it is not sufficient to simply find the ordinary Stokes lines in the problem, but instead we must also determine the higher-order Stokes line behaviour, and therefore where the ordinary Stokes lines are switched on and off. This will permit us to determine the full asymptotic free-surface wave behaviour.

2 Formulation

We consider the problem of unsteady mean flow past a submerged point source in three dimensions, beginning in a prescribed initial flow configuration. We suppose that the strength of the source is small so that the problem may be linearized.

2.1 Full problem

We consider a three-dimensional incompressible, irrotational, inviscid free-surface flow of infinite depth with a submerged point source at depth H and upstream flow velocity U. The steady version of this problem was considered in Lustri & Chapman (2013). We normalise the fluid velocity with U and distance with an unspecified length L, giving non-dimensionalised source depth $h=H/L$, shown schematically in Figure 1. The natural choice for L is H, but we prefer to separate H and L to allow for direct comparison with the results from Lustri & Chapman (2013).

Denoting the (non-dimensional) position of the free surface by $z=\xi(x,y,t)$, the (non-dimensional) velocity potential satisfies

$$\nabla^2\phi=0, \qquad -\infty<z<\xi(x,y,t), \tag{2.1}$$

https://doi.org/10.1017/S0956792514000217 Published online by Cambridge University Press

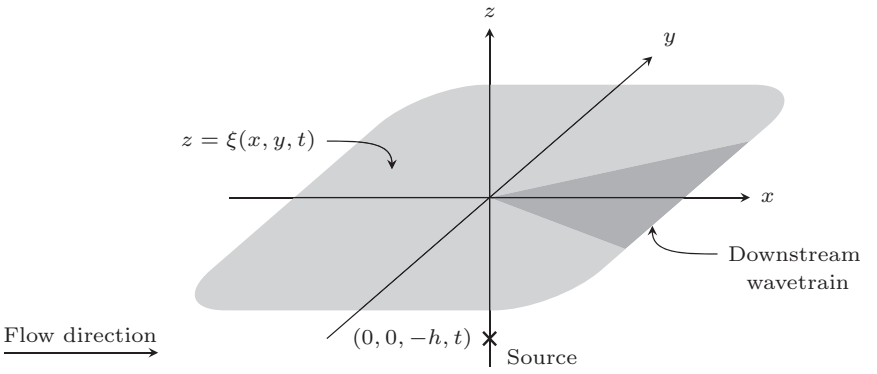

FIGURE 1. Prescribed fluid configuration for three-dimensional flow over a source. The shaded region represents the position of the free surface $\xi(x, y, t)$, and the cross represents the position of the source. The flow region lies below the free surface, and the mean flow is moving from left to right, with flow velocity U in the unscaled problem. A possible downstream wave region is illustrated in darker grey.

with kinematic and dynamic boundary conditions

$$\xi_x \phi_x + \xi_y \phi_y + \xi_t = \phi_z, \qquad z = \xi(x, y, t), \tag{2.2}$$

$$\frac{1}{2}\epsilon(\phi_t + |\nabla\phi|^2 - 1) + \xi = 0, \qquad z = \xi(x, y, t), \tag{2.3}$$

where we have written $\epsilon = F^2$, where

$$F = \frac{U}{\sqrt{gL}} \tag{2.4}$$

is the Froude number, and g is the acceleration due to gravity. We will be concerned with the limit $0 < \epsilon \ll 1$. Since the flow is uniform in the far field, $\phi_x \to 1$ there, while at the source

$$\phi \sim \frac{\delta}{4\pi\sqrt{x^2 + y^2 + (z + h)^2}} \qquad \text{as} \quad (x, y, z, t) \to (0, 0, -h, t). \tag{2.5}$$

We will be concerned with the limit $0 < \delta \ll \epsilon$, so that the disturbance to the free stream is weak and the equations may be linearized in δ. Specifically, if $\delta = o(\epsilon^2)$, higher-order powers of δ can be discarded, as they will not appear in any of the subsequent analysis.

We denote the initial flow conditions, prescribed at $t = 0$, as $\phi = \phi_0$ and $\xi = \xi_0$. For convenience, we set the initial condition to be the leading-order solution to the linearized steady-state problem, found by solving the steady version of (2.7)–(2.10) with $\epsilon = 0$, giving

$$\phi_0 = \frac{\delta}{4\pi\sqrt{x^2 + y^2 + (z + h)^2}} + \frac{\delta}{4\pi\sqrt{x^2 + y^2 + (z - h)^2}}, \qquad \xi_0 = 0. \tag{2.6}$$

This will ensure that in subsequent analysis, the flow is steady at leading order in the low-Froude number limit. Finally, we note that the initial flow state is waveless, and hence prescribe that free surface is always waveless in the far field.

https://doi.org/10.1017/S0956792514000217 Published online by Cambridge University Press

2.2 Linearization

We linearize about uniform flow by setting

$$\phi = x + \delta\overline{\phi}, \qquad \xi = \delta\overline{\xi},$$

to give, at leading order in δ

$$\nabla^2\overline{\phi} = 0, \qquad -\infty < z < 0. \tag{2.7}$$

$$\overline{\phi}_z - (\overline{\xi}_x + \overline{\xi}_t) = 0, \qquad z = 0, \tag{2.8}$$

$$\epsilon(\overline{\phi}_x + \overline{\phi}_t) + \overline{\xi} = 0, \qquad z = 0, \tag{2.9}$$

where the boundary conditions are now applied on the fixed surface $z = 0$. The far-field conditions imply that $\overline{\phi} \to 0$ as $x^2 + y^2 + z^2 \to \infty$, while near the source

$$\overline{\phi} \sim \frac{1}{4\pi\sqrt{x^2 + y^2 + (z + h)^2}} \qquad \text{as} \quad (x, y, z, t) \to (0, 0, -h, t). \tag{2.10}$$

The initial conditions given in (2.6) become

$$\overline{\phi}_0 = \frac{1}{4\pi\sqrt{x^2 + y^2 + (z + h)^2}} + \frac{1}{4\pi\sqrt{x^2 + y^2 + (z - h)^2}}, \qquad \overline{\xi}_0 = 0. \tag{2.11}$$

Finally, we analytically continue the free surface such that $x, y \in \mathbb{C}$, with the free surface still defined as the surface satisfying $z = 0$. This does not change the form of equations (2.7)–(2.10), but it does mean that the two-dimensional physical free surface is a subset of a four-dimensional complexified free surface.

2.3 Series expression

Following the approach of Chapman & Vanden-Broeck (2006), we first expand the fluid potential and free-surface position as a power series in ϵ,

$$\overline{\phi} \sim \sum_{n=0}^{\infty} \epsilon^n \phi^{(n)}, \qquad \overline{\xi} \sim \sum_{n=0}^{\infty} \epsilon^n \xi^{(n)} \tag{2.12}$$

to give for $n \geqslant 0$

$$\nabla^2\phi^{(n)} = 0, \qquad -\infty < z < 0, \tag{2.13}$$

$$\phi_z^{(n)} - \left[\xi_x^{(n)} + \xi_t^{(n)}\right] = 0, \qquad z = 0, \tag{2.14}$$

$$\left[\phi_x^{(n-1)} + \phi_t^{(n-1)}\right] + \xi^{(n)} = 0, \qquad z = 0, \tag{2.15}$$

with the convention that $\phi^{(-1)} = 0$. The far-field behaviour tends to zero at all orders of n and the singularity condition (2.10) is applied to the leading-order expression, giving

$$\phi^{(0)} \sim \frac{1}{4\pi\sqrt{x^2 + y^2 + (z + h)^2}} \qquad \text{as} \quad (x, y, z, t) \to (0, 0, -h, t).$$

https://doi.org/10.1017/S0956792514000217 Published online by Cambridge University Press

As the initial condition (2.11) is the leading-order steady state solution, the leading-order behaviour remains steady and is given by

$$\phi^{(0)} = \frac{1}{4\pi\sqrt{x^2+y^2+(z+h)^2}} + \frac{1}{4\pi\sqrt{x^2+y^2+(z-h)^2}}, \qquad \xi^{(0)} = 0.$$

This formulation illustrates clearly why the small ϵ limit is singular in this problem. We see from (2.14) and (2.15) that the time derivative of $\xi^{(n)}$ is used to determine $\phi^{(n)}$, and the time derivative from $\phi^{(n)}$ is subsequently used to determine $\xi^{(n+1)}$. As these derivatives of $\xi^{(n)}$ and $\phi^{(n)}$ are calculated only once the terms themselves have been determined, this expansion removes the time-evolutionary behaviour of the unsteady problem. The removal of this behaviour in the small ϵ limit produces the singular nature of the limit, and hence the unsteady exponentially-small terms identified in Section 3.1.

3 Late-order terms

In order to optimally truncate the asymptotic series prescribed in (2.12), we must determine the form of the late-order terms. We therefore make the factorial-over-power ansatz (Chapman *et al.* (1998))

$$\phi^{(n)} \sim \frac{\Phi(x,y,z,t)\Gamma(n+\gamma)}{\chi(x,y,z,t)^{n+\gamma}}, \qquad \xi^{(n)} \sim \frac{\Xi(x,y,t)\Gamma(n+\gamma)}{\chi(x,y,0,t)^{n+\gamma}}, \qquad \text{as} \quad n \to \infty, \tag{3.1}$$

where γ is constant.

Each late-order contribution is associated with a singularity in the early terms of the asymptotic expansions (2.12) on the analytically-continued free surface at which $\chi = 0$. The position of these singularities will be discussed in Sections 3.1.1 and 3.1.2.

It is important to note that the expression for $\xi^{(n)}$ is restricted to $z = 0$, as it describes the free-surface position. This does not pose a problem for the subsequent analysis, but does ensure that care must be taken at each stage to determine whether we are considering the full flow region, or only the free surface.

3.1 Calculating the singulant

Applying the ansatz expressions in (3.1) to the governing equation (2.13) and taking the first two orders as $n \to \infty$ gives

$$\chi_x^2 + \chi_y^2 + \chi_z^2 = 0, \tag{3.2}$$

$$2\Phi_x\chi_x + 2\Phi_y\chi_y + 2\Phi_z\chi_z = -(\chi_{xx} + \chi_{yy} + \chi_{zz}), \tag{3.3}$$

while the boundary conditions (2.14) and (2.15) become at leading order

$$-(\chi_x + \chi_t)\Phi + \Xi = 0, \qquad z = 0, \tag{3.4}$$

$$-\chi_z\Phi + (\chi_x + \chi_t)\Xi = 0, \qquad z = 0. \tag{3.5}$$

This system of equations has non-zero solutions when

$$(\chi_x + \chi_t)^2 = \chi_z. \tag{3.6}$$

https://doi.org/10.1017/S0956792514000217 Published online by Cambridge University Press

Combining this result with (3.2) gives the eikonal equation on the free surface as

$$(\chi_x + \chi_t)^4 + \chi_x^2 + \chi_y^2 = 0. \tag{3.7}$$

In order to determine the form of the prefactors Φ and Ξ, we must solve (3.3). This involves writing the equation in a way that it may be solved on the free surface, and showing that the resultant behaviour contains identical characteristics to the eikonal equation. This information about the ray structure may be used to obtain an integral form for Φ, and hence Ξ. We omit the prefactor calculations here, however the procedure is very similar to that described by Lustri & Chapman (2013).

3.1.1 *Steady singularity*

The leading-order solution (2.3) is singular (and hence $\chi = 0$) at points satisfying

$$x^2 + y^2 + (z \pm h)^2 = 0,$$

where the sign chosen depends upon which of the two singularities is being considered. For complex values of x, y and z, this defines a four-dimensional hyper-surface. Irrespective of which singularity is under consideration, this hyper-surface intersects the four-dimensional complexified free surface on the two-dimensional hyper-surface satisfying $x^2+y^2+h^2=0$.

The eikonal equation may be solved using Charpit's method (Ockendon *et al.*, 1999). In fact, comparing this Charpit system to the equivalent analysis for the steady problem performed in Lustri & Chapman (2013), we see that the solution for χ is identical in both cases, giving

$$\chi = \frac{2h^4 u}{s^4}, \qquad \text{where} \qquad u = \pm\frac{h^3(s-x)}{s(2h^2+s^2)},$$

and s is one of the four solutions to

$$\left(x^2+y^2\right)s^4 + 4xh^2s^3 + \left(h^2x^2 + 4h^2y^2 + 4h^4\right)s^2 + 4h^4xs + \left(4y^2h^4 + 4h^6\right) = 0.$$

Following Lustri & Chapman (2013), we may discard four of the eight solutions immediately, as they would produce exponentially-large waves on the free surface. The remaining four contributions are denoted as $\chi_{L1,2}$ and $\chi_{T1,2}$, associated with longitudinal and transverse waves respectively, and are illustrated in Figure 2.

For more details on determining the behaviour and interaction between the longitudinal and transverse wave contributions, see Lustri & Chapman (2013). This study demonstrated that longitudinal waves are switched on by the leading-order behaviour across a Stokes line following $x=0$, while the transverse waves were subsequently switched on by the longitudinal wave behaviour along wedge-like curves that tend to the Kelvin wedge Kelvin (1887) in the limit that $h \to 0$. This behaviour is illustrated in Figure 3.

3.1.2 *Unsteady singularity*

There is a second class of singularity present on the complexified free surface due to the initial discontinuous disturbance in the system. In Appendix A we show that the

https://doi.org/10.1017/S0956792514000217 Published online by Cambridge University Press

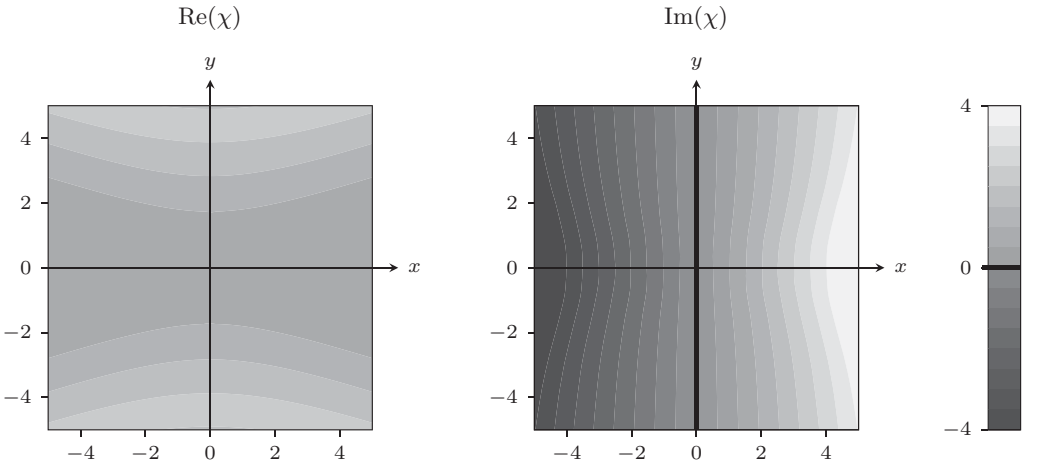

(a) Behaviour of χ_{L1}

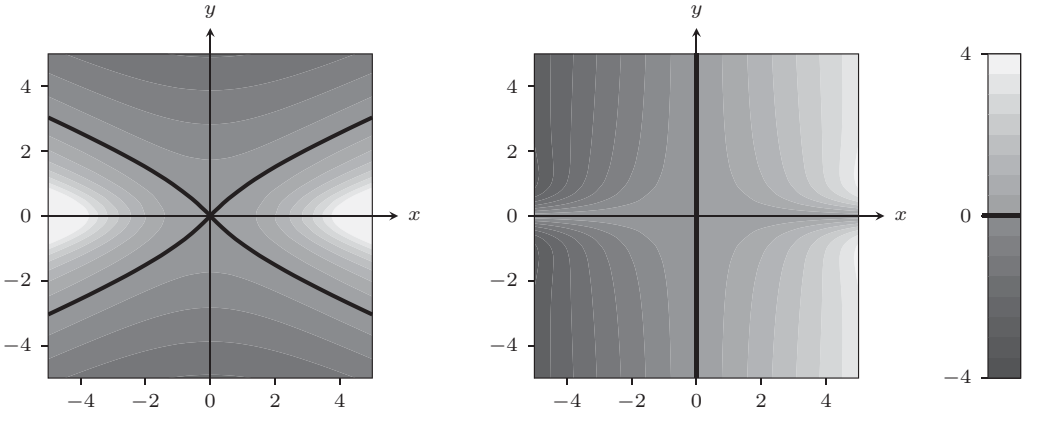

(b) Behaviour of χ_{T1}

FIGURE 2. Singulants obtained by solving (3.7) with boundary data given by $\chi = 0$ on the curve described in (3.1.1). The behaviour of χ_{L2} and χ_{T2} are given by the complex conjugates of these solutions.

series (2.12) contains terms which are singular when $t = 0$. These terms exist due to the instantaneous change in the system that occurs at $t = 0$. Prior to this point in time, the surface is held in a fixed position, while afterwards, it is permitted to vary freely.

In a similar analysis to that performed by Chapman & Mortimer (2005), we see that simply applying the condition $\chi = 0$ at $t = 0$ is not sufficient to uniquely determine χ, as the rays never leave the boundary data. Instead, we specify that all of the singulant rays must originate at the source or its reflection, located at $(x, y, z) = (0, 0, \pm h)$, when $t = 0$.

In fact, this solution will be radially symmetric about the point $x = t$. Hence, for simplicity, we rewrite (3.7) in terms of time and the radial distance from this point,

https://doi.org/10.1017/S0956792514000217 Published online by Cambridge University Press

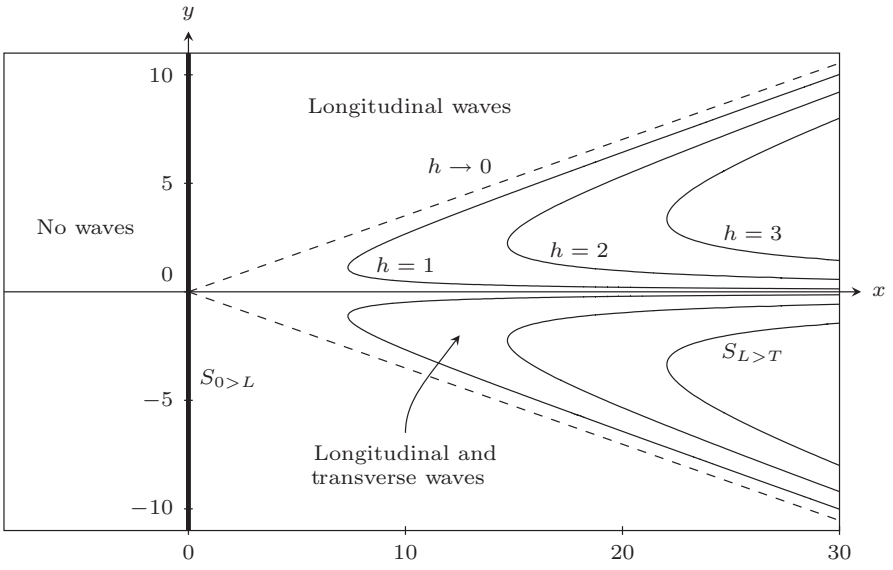

FIGURE 3. Stokes lines associated with steady-state flow behaviour, obtained in Lustri & Chapman (2013) and also present in the unsteady problem. The bold curve represents the Stokes line across which downstream longitudinal waves associated with $\chi_{L1,2}$ are switched on. The narrow curves represent the Stokes lines across which downstream transverse waves associated with $\chi_{T1,2}$ are switched on, for a range of values of h. For more details, see Lustri & Chapman (2013).

$\rho = \sqrt{(x-t)^2 + y^2}$. This gives the eikonal equation as

$$\chi_t^4 + \chi_\rho^2 = 0,$$

with the condition that $\chi = 0$ at $\rho = -h^2$.

Again using Charpit's method to solve this equation, we find the solutions

$$\chi_{U1} = \frac{t^2}{4\,(h - \mathrm{i}\rho)}, \qquad \chi_{U2} = \frac{t^2}{4\,(h + \mathrm{i}\rho)}. \tag{3.8}$$

As with the steady singularity, there exist other solutions to this system (specifically $-\chi_{U1}$ and $-\chi_{U2}$); however, these contributions would produce exponentially large free-surface behaviour, as $\mathrm{Re}(\chi) < 0$ on the entire physical free surface. Consequently, on physical grounds we may conclude that these remaining singulant contributions are inactive. We also note that χ_{U2} is the complex conjugate of χ_{U1}.

In Figure 4, we see that each of these singulants satisfies $\mathrm{Im}(\chi) = 0$ at the point $x = t$ only, and has $\mathrm{Re}(\chi) > 0$ everywhere. Hence they produce free-surface behaviour that is either active everywhere or inactive everywhere on the free surface. Noting that these are the only late-order contributions to contain any unsteady behaviour, we conclude that these contributions must be present on the free surface for there to be any unsteady free-surface wave behaviour. Furthermore, as the phase of the resultant free-surface wave

https://doi.org/10.1017/S0956792514000217 Published online by Cambridge University Press

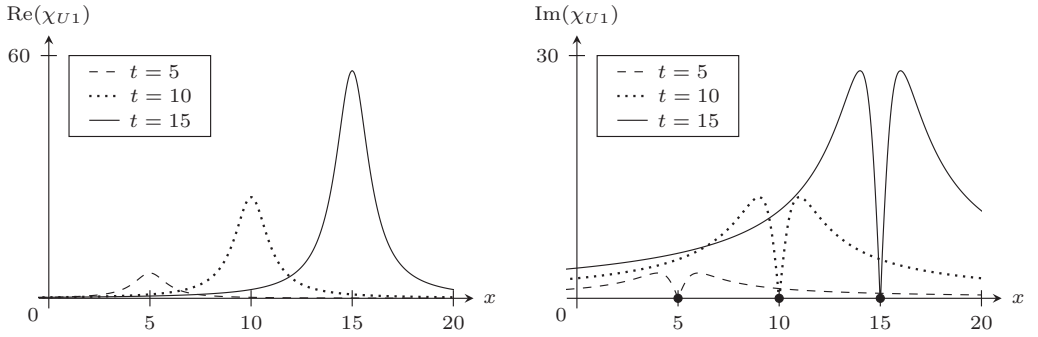

(a) Re(χ_{U1}) (b) Im(χ_{U1})

FIGURE 4. Plots of the real and imaginary parts of χ_{U1} with $h = 1$ over a range of x for $y = 0$ and various t values. Furthermore, we recall that χ_{U1} is radially symmetric about the point $x = t$. Hence, the singulant expression satisfies $\mathrm{Im}(\chi) = 0$ only at $x = t$, indicated by a black circle, while $\mathrm{Re}(\chi) > 0$ on the entire free surface. Noting that χ_{U2} is the complex conjugate of χ_{U1}, we determine that the free-surface contributions associated with these two contributions are always exponentially small on the free surface, and take the form of an expanding ripple centred on $x = t$.

is given by $\mathrm{Im}(\chi)$, we see that the unsteady free-surface behaviour takes the form of an expanding ripple centred on $x = t$, and hence propagates with the flow.

4 Complete Stokes structure

We recall from the analysis of the steady problem (Lustri & Chapman, 2013) that the steady free-surface behaviour contains longitudinal waves (associated with $\chi_{L1,2}$) that are switched on by the leading-order behaviour along curves satisfying $\mathrm{Im}(\chi_{L1,2}) = 0$, and transverse waves (associated with $\chi_{T1,2}$) that are switched on by the longitudinal wave behaviour along curves satisfying $\mathrm{Im}(\chi_{L1,2}) = \mathrm{Im}(\chi_{T1,2})$. We will concentrate only on χ_{U1}, χ_{L1} and χ_{T1}, noting that the interaction between the remaining contributions will be identical, as they take appropriate complex conjugate values.

Figure 3 illustrates the regions in which the respective steady-state contributions are active in the absence of unsteady free-surface behaviour. The Stokes lines indicated in Figure 3 are denoted by $S_{L>T}$ and $S_{0>T}$, with the inequality indicating which of the two contributions is exponentially dominant, with L, T and 0 denoting the longitudinal wave contribution, the transverse wave contribution and the leading-order behaviour respectively. This convention will be used for the remainder of the current investigation, where the letter U will be used to refer to the unsteady ripple contribution.

Thus far, we have considered the Stokes switching between the base flow and the steady and unsteady waves separately. To complete the picture, we need to consider Stokes interaction between the steady and unsteady wave contributions. This involves determining the curves that satisfy $\mathrm{Im}(\chi_{U1}) = \mathrm{Im}(\chi_{L1})$ and $\mathrm{Im}(\chi_{U1}) = \mathrm{Im}(\chi_{T1})$, as well as considering the effect of higher-order Stokes lines, as discussed in Chapman & Mortimer (2005); Howls *et al.* (2004).

https://doi.org/10.1017/S0956792514000217 Published online by Cambridge University Press

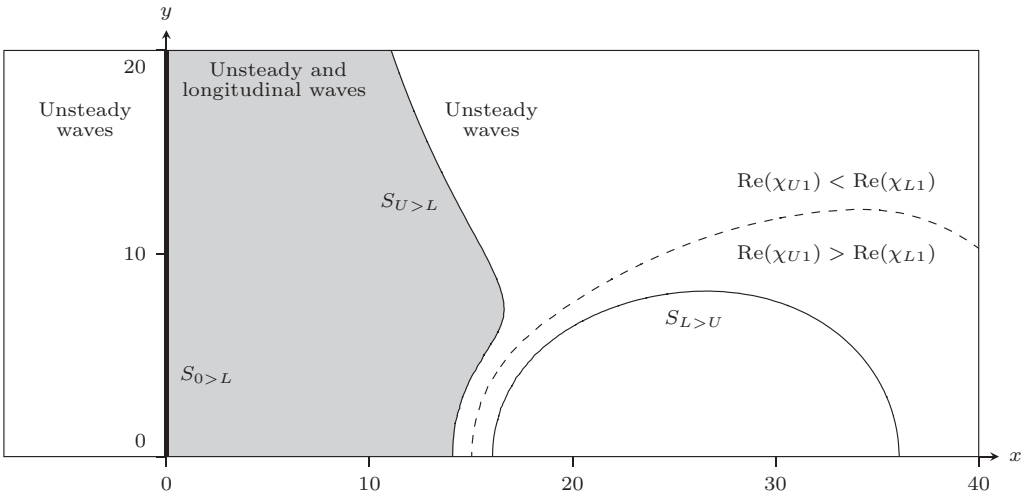

FIGURE 5. This figure illustrates Stokes and anti-Stokes lines caused by interactions between the late-order terms corresponding to χ_{L1} and χ_{U1} for $t = 30$ and $h = 1$. The thin unbroken curves indicate Stokes lines across which $\mathrm{Im}(\chi_{L1}) = \mathrm{Im}(\chi_{U1})$, while the thick unbroken curve represents the Stokes line across which $\mathrm{Im}(\chi_{L1}) = 0$. The dashed line indicates an anti-Stokes line across which $\mathrm{Re}(\chi_{L1}) = \mathrm{Re}(\chi_{U1})$. The unsteady free-surface contribution associated with χ_{U1} is always active. The longitudinal waves are switched on across the line $x = 0$ by the leading-order behaviour. Here, we find that this behaviour is switched off by the unsteady contribution as $S_{U>L}$ is crossed. $S_{L>U}$ must be inactive, as the longitudinal contribution is absent in this region, and therefore cannot switch the unsteady contribution. Hence, the longitudinal waves are present only in the shaded region of the free surface. An identical figure would be obtained by considering interactions between χ_{L2} and χ_{U2}

4.1 Longitudinal waves

We first consider the interaction between the unsteady surface ripple and the longitudinal waves, as this behaviour may be investigated without considering the transverse wave behaviour.

In Figure 5, we show the curves along which χ_{L1} and χ_{U1} have equal real or imaginary parts, giving the location of anti-Stokes lines and Stokes lines respectively. From this figure, we see that there are two potential Stokes lines on the free surface, separated by an anti-Stokes line.

On the left-hand side of the anti-Stokes line, $\mathrm{Re}(\chi_{L1}) > \mathrm{Re}(\chi_{U1})$, implying that the longitudinal wave behaviour is exponentially sub-dominant compared to the unsteady behaviour. Recalling that sub-dominant effects are switched across a Stokes line, we find that longitudinal waves are switched on across $S_{U>L}$. However, on the right-hand side of the anti-Stokes line, $\mathrm{Re}(\chi_{U1}) > \mathrm{Re}(\chi_{L1})$, and hence the longitudinal wave behaviour would exponentially dominate the unsteady wave behaviour. However, as the longitudinal waves are not present, no switching may occur across $S_{L>U}$, and it is therefore inactive.

We therefore conclude that longitudinal waves are switched on across the Stokes line along $x = 0$ as in Section 3.1.1, and switched off as $S_{U>L}$ is crossed from left to right. Figure 6 illustrates the wave region for a range of values of t with $h = 1$. We see that the wavefront tends to $x \to \infty$ as $t \to \infty$. In fact, by comparing the behaviour of χ_{L1} and

https://doi.org/10.1017/S0956792514000217 Published online by Cambridge University Press

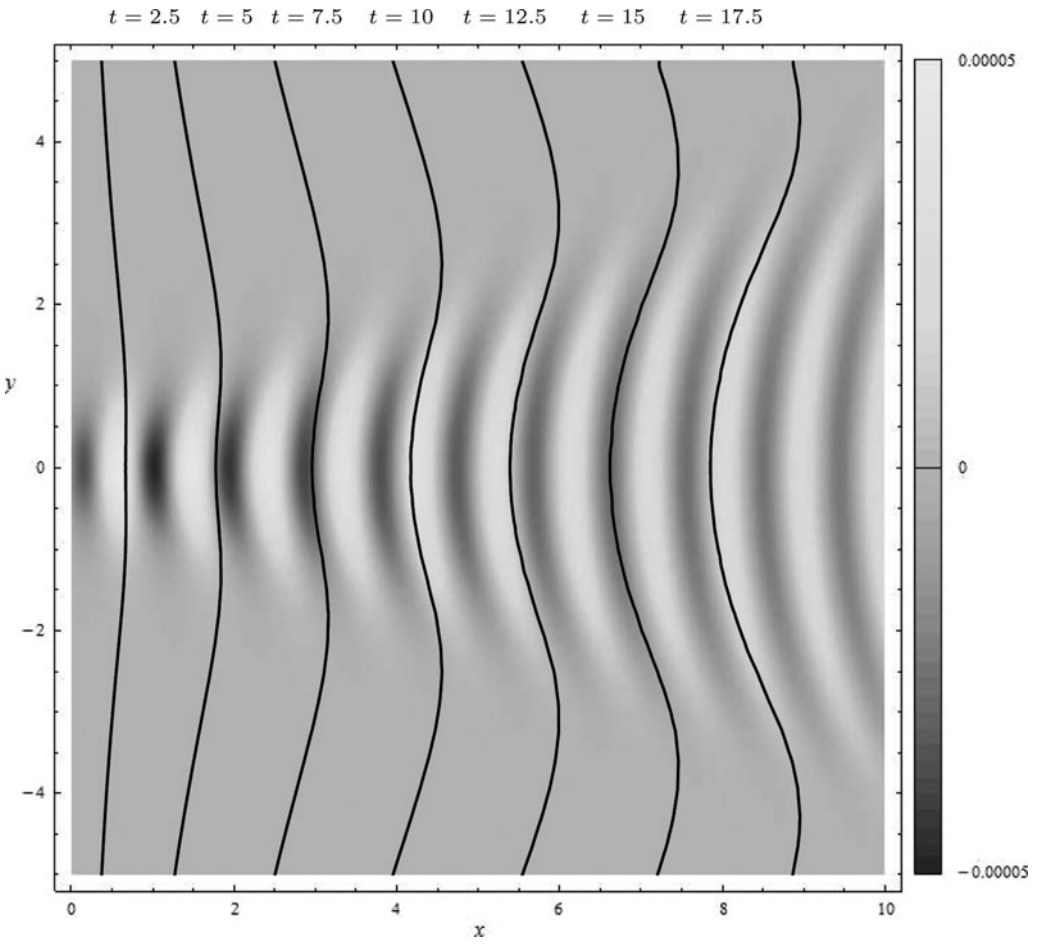

FIGURE 6. Position of the Stokes line associated with the longitudinal wavefront as t is varied, shown as bold curves. The steady free-surface longitudinal waves, with amplitudes calculated in Lustri & Chapman (2013), are shown; however, only those to the left of the wavefront at a given time are present on the surface in the unsteady case. We also note that the waves are switched on across the curve $x = 0$ for all time.

χ_{U1} as $x \to \infty$, it may be seen that the position of the wavefront along the curve $y = 0$ (denoted x_f) is given by

$$x_f \sim \frac{t}{2} - h \qquad \text{as } t \to \infty.$$

It is also simple to show that $x_f \to 0^+$ in the limit that $y \to \pm\infty$ for fixed t.

4.2 Transverse waves

Determining the unsteady behaviour of the free-surface transverse waves is more complicated, as they may interact with both the unsteady free-surface behaviour and the steady longitudinal free-surface waves. We expect that as $t \to \infty$, the behaviour of the transverse

https://doi.org/10.1017/S0956792514000217 Published online by Cambridge University Press

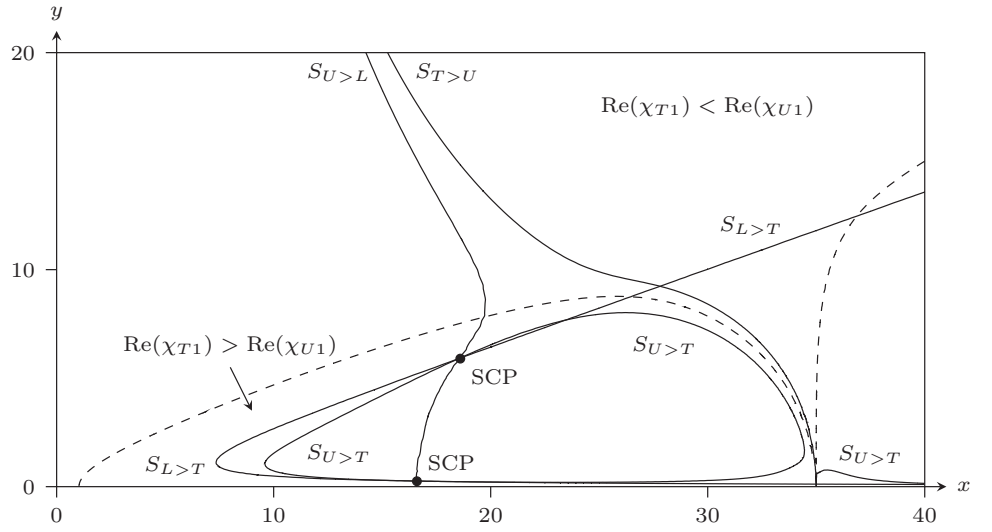

FIGURE 7. Possible Stokes lines on the free surface for unsteady flow over a source of depth $h = 1$ at $t = 35$. The solid curves represent Stokes lines, while the dashed curve represents a relevant anti-Stokes line, along which $\mathrm{Re}(\chi_{T1}) = \mathrm{Re}(\chi_{U1})$. Stokes crossing points (where all three Stokes lines intersect) are denoted by circles. The steady free-surface transverse-wave contribution associated with χ_{T1} can only be switched on by the unsteady free-surface contribution associated with χ_{U1} when $\mathrm{Re}(\chi_{T1}) > \mathrm{Re}(\chi_{U1})$, and hence $S_{T>U}$ cannot be active. The Stokes line indicated by $S_{L>U}$ in Figure 5 has been omitted, as well as any related Stokes crossing points, as it does not contribute to the surface behaviour.

waves will tend to the steady-state behaviour described in Lustri & Chapman (2013) and illustrated in Figure 3.

In Figure 7, we illustrate all of the potential Stokes lines involving the transverse wave contribution for $t = 35$ and $h = 1$, as well as relevant anti-Stokes lines. We recall that the unsteady contribution is present everywhere on the free surface, while the longitudinal wave contribution is present only to the left of the Stokes line caused by the interaction between the two. The Stokes line across which transverse waves are switched by longitudinal waves is identical to that obtained in the steady case found in Lustri & Chapman (2013). There are two possible Stokes lines across which transverse waves may be switched by the unsteady behaviour. However, as in the longitudinal case, these two possible Stokes lines are separated by an anti-Stokes line. By comparing the real parts of the singulants in each of these regions, we see that the unsteady behaviour may only switch the transverse wave behaviour on the left-hand side of the anti-Stokes line, where it is exponentially sub-dominant compared to the unsteady ripple.

In Figure 7, there are two Stokes crossing points, at which all three Stokes lines intersect. There is a higher-order Stokes line passing through these points, satisfying

$$\mathrm{Im}\left[\frac{\chi_{U1} - \chi_{L1}}{\chi_{U1} - \chi_{T1}}\right] = 0. \tag{4.1}$$

In order for the transverse waves to be switched in such a fashion that they do not

https://doi.org/10.1017/S0956792514000217 Published online by Cambridge University Press

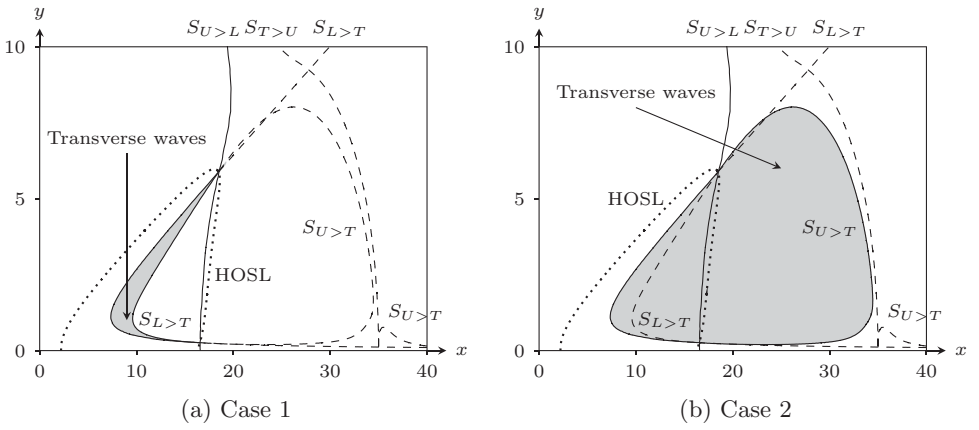

FIGURE 8. The region of the free surface in Figure 7 containing transverse waves must be either (a) Case 1 or (b) Case 2. These are the only possibilities that restrict the transverse waves to a finite region of the free surface and tend to the steady behaviour obtained in Lustri & Chapman (2013) as $t \to \infty$. In each case, active Stokes lines are represented as solid curves, while relevant inactive Stokes lines are shown as dashed curves. The higher-order Stokes line satisfying (4.1) is illustrated as a dotted curve.

produce exponentially small free-surface waves, occupy a finite region of the free surface, and tend to the steady solution as $t \to \infty$, some of the Stokes lines in the problem must switch off across the higher-order Stokes line (Howls *et al.*, 2004; Chapman & Mortimer, 2005). Hence, the region of the free-surface containing transverse waves must be either that shown in Figure 8(a) or (b), where the position of the higher-order Stokes line is also indicated.

To determine which of these cases is correct, we set $\mathrm{Re}(y) = 3$ and examine the Stokes behaviour when y is permitted to take complex values, shown in Figure 9. We see that if the second case is true, the Stokes line in Figure 10 on the right-hand side of the anti-Stokes line must be active, which is not possible as it leads to exponentially large waves on the free surface, as discussed in Figure 7. Hence, transverse waves are restricted to the region illustrated in Figure 8(a).

Finally, in Figure 10 we illustrate the behaviour of this region as t increases. The transverse wave region clearly expands over time, and does tend to the steady state behaviour obtained in Lustri & Chapman (2013).

5 Numerical comparison

A number of sample surface profiles along $y = 0$ may be seen in Figure 11. These were computed by formulating the solution to the linearized problem described in (2.7)–(2.11) in terms of an integral which was subsequently evaluated numerically. Details of the numerical procedure are given in Appendix B.

In Figure 11, we compare the position of the longitudinal wavetrain with the behaviour predicted by the asymptotic solution. In Section 4.1, we predicted that the longitudinal waves would switch off across a Stokes line that intersects the free surface, in an inner

https://doi.org/10.1017/S0956792514000217 Published online by Cambridge University Press

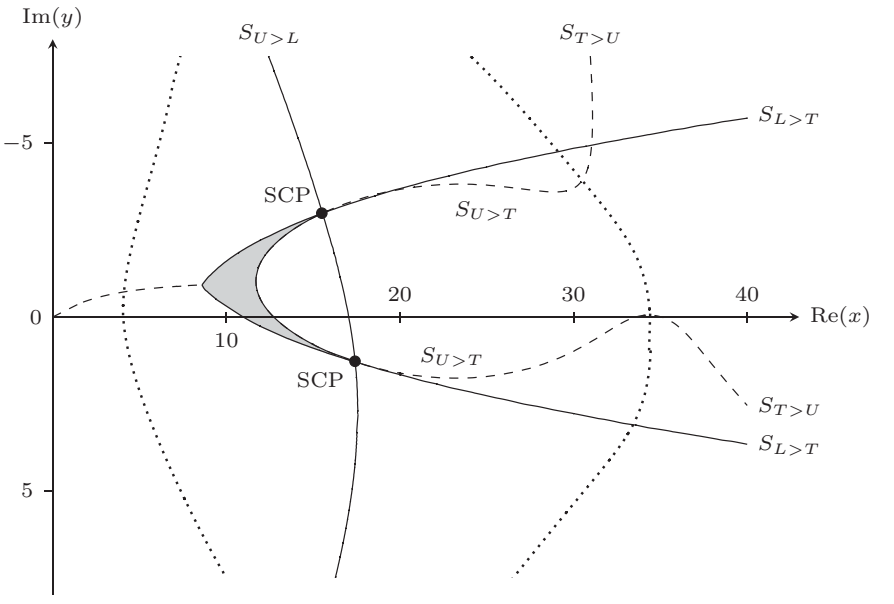

FIGURE 9. Stokes structure on the complexified free surface associated with Figure 7, along the curve $y = 3$. Solid curves represent active Stokes lines, whereas dashed curves represent inactive Stokes lines. The dotted curve represents an anti-Stokes line along which $\mathrm{Re}(\chi_{U1}) = \mathrm{Re}(\chi_{T1})$. Black circles represent the Stokes crossing points at which Stokes lines are switched off. The two Stokes lines indicated in Figure 7 as $S_{U>T}$ and $S_{T>U}$ are shown to be connected, and hence must either both be active, or both be inactive. If they are both active, then the Stokes line labelled $S_{T>U}$ in Figure 7, which is not possible. Hence, we conclude that $S_{U>T}$ is active only on the left of the Stokes crossing points. This corresponds to Case 1 in Figure 8. Finally, the Stokes lines following $S_{L>T}$ intersect at a caustic, from which an inactive Stokes line originates.

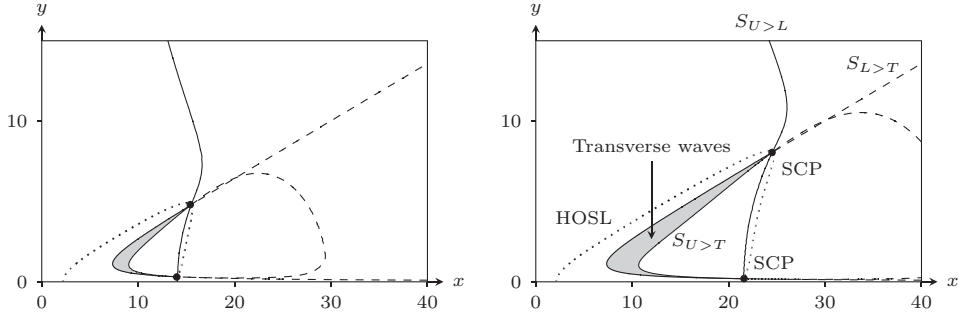

FIGURE 10. The region of the free-surface containing an exponentially small transverse wave contribution as t is varied. Transverse waves are present in the shaded regions only.

https://doi.org/10.1017/S0956792514000217 Published online by Cambridge University Press

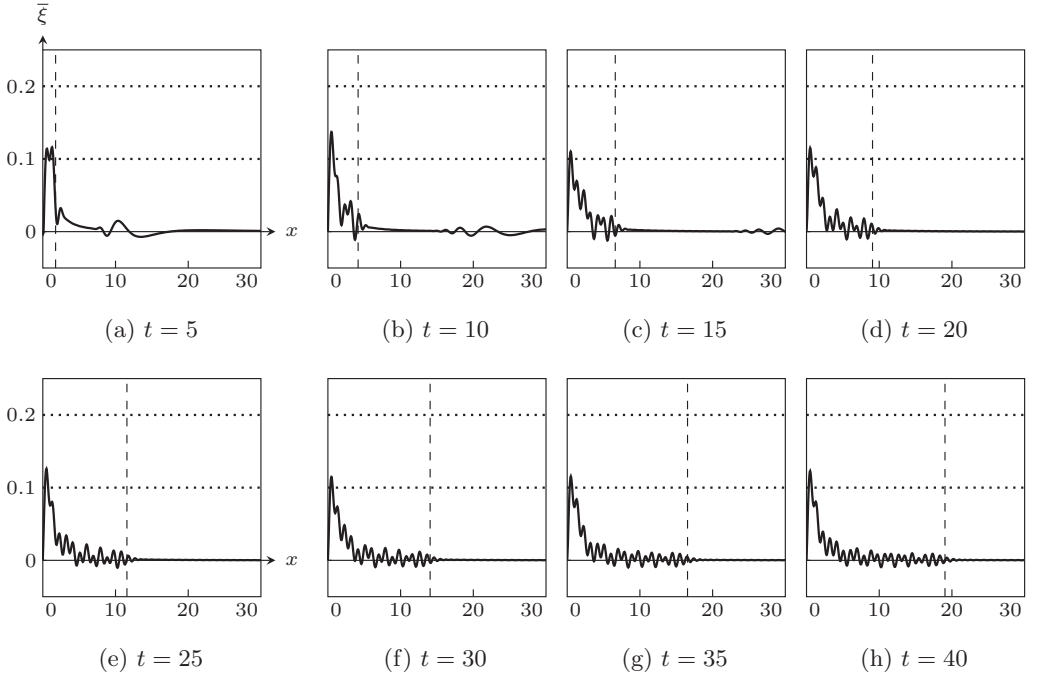

FIGURE 11. Comparison between the numerically-obtained free surface for flow over a source of depth $h = 1$ with $\epsilon = 0.15$ and the position of the wavefront predicted using exponential asymptotic analysis. The dashed line indicates the point at which the Stokes line intersects the free surface along $y = 0$. The asymptotic analysis predicts that the longitudinal waves are switched off smoothly in a region of width $\mathcal{O}(\epsilon^{1/2})$ as this point is crossed. The computed wavefront agrees strongly with the asymptotic results. Additionally, the unsteady wave behaviour, which takes the form of a ripple centred on $x = t$, is clearly visible in (a)–(c).

region with width of $\mathcal{O}(\epsilon^{1/2})$. The point at which this Stokes line intersects the free surface is indicated in Figure 11 by a dashed line. We see that there is a strong agreement between the asymptotic prediction for the position of the propagating wavefront and that obtained in the numerical solution.

Additionally, in Figure 11(b) we have labelled the unsteady contribution, which takes the form of an expanding ripple which is radially symmetric about $x = t$. As the ripple is expanding at the same rate at which the centre is propagating downstream, we see that the forward edge of the ripple moves downstream at twice the flow velocity, while the backward edge remains above $x = 0$. It is this backward edge of the unsteady ripple that produces the slight irregularities in the downstream wavetrain, however these irregularities vanish as $t \to \infty$.

Finally, in Figure 12, we illustrate the numerically-obtained free-surface behaviour for flow over a source with depth $h = 0.5$ and $\epsilon = 0.15$, at $t = 20$. Both longitudinal and transverse waves are visible in this figure. While it is difficult to directly compare the transverse wave behaviour to asymptotic calculations, due to their exponential sub-dominance even to longitudinal wave effects, it is clear that they demonstrate the same propagating wing-like structure seen in Figure 10. We see that the waves do not extend infinitely

https://doi.org/10.1017/S0956792514000217 Published online by Cambridge University Press

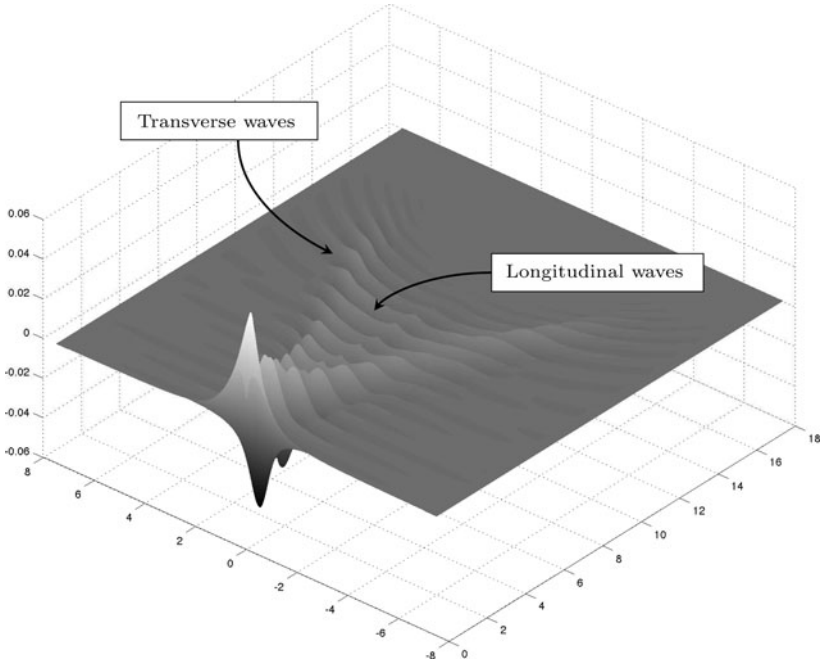

FIGURE 12. Example free-surface profile for $\epsilon = 0.15$ and $h = 0.5$ at $t = 20$, calculated on increments of $\Delta x = \Delta y = 0.1$. Both longitudinal and transverse wave effects are visible, as indicated on the figure. The position of the wavefront is apparent, and this is consistent with the Stokes structure and asymptotic behaviour calculated in Section 4.

downstream, but instead there is a visible wavefront beyond which no longitudinal or transverse waves exist, which is consistent with the asymptotic behaviour determined in Section 4.

6 Discussion and conclusions

In this investigation, we determined the behaviour of unsteady waves on the free surface of flow over a point source in three dimensions in the low-Froude number limit, starting from an initially waveless configuration. These results were compared with the equivalent steady problem, studied in Lustri & Chapman (2013).

We set the initial condition to be waveless, allowing us to investigate the manner in which the steady longitudinal and transverse waves spread along the free surface. In our analysis, we considered the source to be weak, and therefore linearized the problem about the undisturbed solution. We subsequently applied the exponential asymptotic techniques of Chapman *et al.* (1998); Chapman & Mortimer (2005); Olde Daalhuis *et al.* (1995) in order to determine the behaviour of the resultant gravity waves on the surface of the flow.

In the analysis of the steady problem, Lustri & Chapman (2013) found that longitudinal waves were present in the entire right-half plane, while that transverse waves were located within wedge-shaped regions on either side of the curve $y = 0$. In the unsteady problem, we found that a third exponentially sub-dominant contribution was present on the free surface, representing the transient ripple caused by the initial disturbance at $t = 0$.

https://doi.org/10.1017/S0956792514000217 Published online by Cambridge University Press

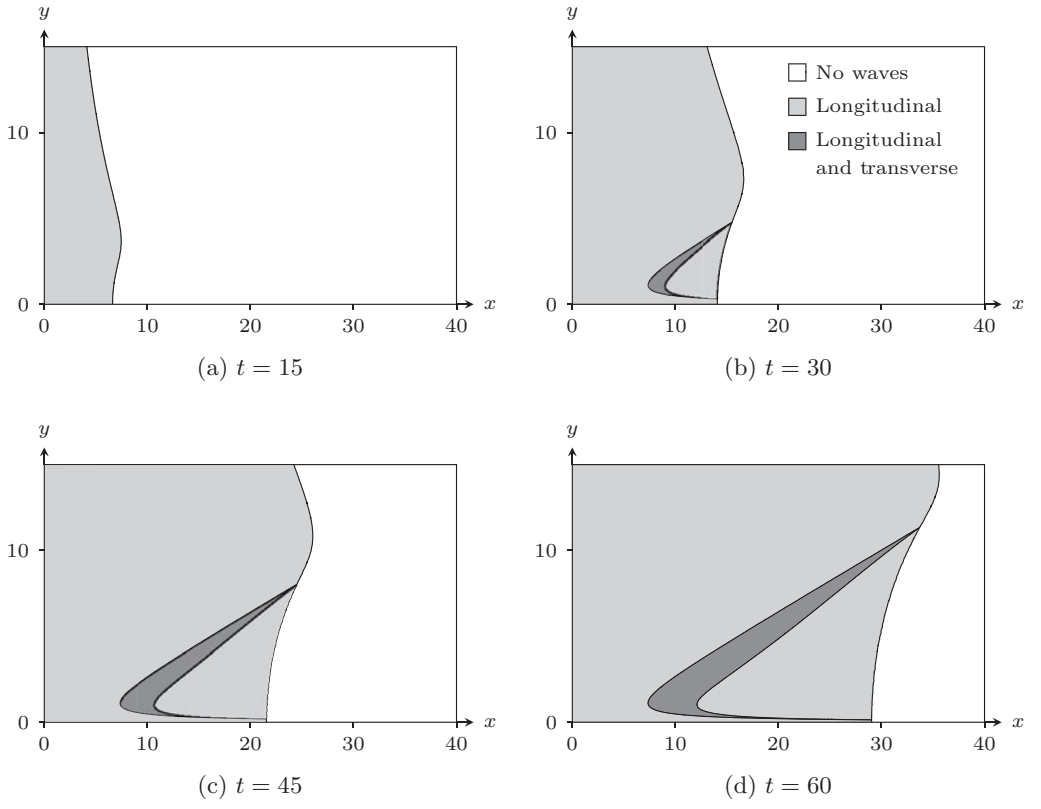

FIGURE 13. Regions on the free surface containing waves for a range of values of t, for flow past a source of depth $h = 1$. Longitudinal waves are present in the light grey regions, while both longitudinal and transverse waves are present in the darker grey regions.

By comparing the singulants of the unsteady, longitudinal and transverse wave behaviours, we were able to determine the region surface on which the longitudinal and transverse waves were present at any point in time. Determining the region in which longitudinal waves are present simply involved finding the Stokes line associated with the interaction between the unsteady and longitudinal contributions. However, determining the region in which transverse waves are present was more complicated, and required the calculation of a higher-order Stokes line in order to determine which potential Stokes lines are active in the free-surface behaviour. Importantly, we found that both the longitudinal and transverse wave regions tend to the expected steady-state behaviour as $t \to \infty$. Figure 13 illustrates these wave regions over a range of values for t.

Finally, we compared the position of the longitudinal wavefront along $y = 0$ predicted by the asymptotics with numerical solutions to the unsteady flow problem. The numerical solutions were obtained by formulating an integral expression for the surface behaviour and computing the solution to the integrals, and showed good agreement between the asymptotic and numerical results.

In the future, it would be interesting to investigate other linearized geometries, such as flow past a finite line source or a narrow submerged obstruction, considering both the

https://doi.org/10.1017/S0956792514000217 Published online by Cambridge University Press

steady and unsteady problem in each case. Furthermore, there are other flow regimes to which exponential asymptotic methods can be applied; studies have shown that exponential asymptotics may be used to determine the free-surface wave behaviour of capillary waves with small Bond number (Chapman & Vanden-Broeck, 2002), as well as gravity-capillary waves with small Bond and Froude numbers (Trinh & Chapman, 2013a,b). We note that these studies considered only steady two-dimensional problems, and it would interesting to consider the behaviour of these waves in unsteady or three-dimensional regimes.

We also note that it is possible that an asymptotic study of the double integral formulation of the problem, such as that given in the appendices, could reproduce the asymptotic results found in this investigation. However, care must be taken when applying techniques such as contour deformation in multiple integral settings, and the approach followed in the main text has the advantage of being applicable to problems with no convenient integral formulation.

Acknowledgements

This research was supported by the Clarendon Fund, and Australian Laureate Fellowship Grant #FL120100094 from the Australian Research Council.

Appendix A Unsteady singularity

In order for the system to exhibit unsteady behaviour, we note that there must be another singularity that is not immediately apparent in the leading-order behaviour. To find this contribution, we consider a simpler problem; that of the equivalent homogeneous system without a source condition, which we may solve using standard Fourier methods. This allows us to isolate the effect of the initial disturbance on the flow, and specifically to determine the associated singular behaviour. To emphasise this distinction, we will formulate this problem in terms of $\hat{\phi}$ and $\hat{\xi}$, where these are governed by the linearized system

$$\nabla^2\hat{\phi} = 0, \qquad -\infty < z < 0. \tag{A 1}$$

$$\hat{\phi}_z - (\hat{\xi}_x + \hat{\xi}_t) = 0, \qquad z = 0, \tag{A 2}$$

$$\epsilon(\hat{\phi}_x + \hat{\phi}_t) + \hat{\xi} = 0, \qquad z = 0, \tag{A 3}$$

and $\hat{\phi}$ decays in the far field of the domain. This is identical to the system presented in (2.7)–(2.9). However, instead of prescribing a source condition such as (2.10), we set the initial conditions on the free surface $z = 0$ by

$$\phi_0 = \frac{1}{2\pi\sqrt{x^2 + y^2 + h^2}}, \qquad \xi_0 = 0. \tag{A 4}$$

We therefore have identical initial conditions to the system described in Section 2. Taking the Fourier transform in x and y, where k and l are the corresponding Fourier variables,

https://doi.org/10.1017/S0956792514000217 Published online by Cambridge University Press

of the governing equation (A 1) gives

$$\overline{\overline{\phi}}_z - \rho^2 \overline{\overline{\phi}} = 0,$$

where $\rho = \sqrt{k^2 + l^2}$ and two bars denotes taking the double Fourier transform. Noting that $\overline{\overline{\phi}}$ decays as $z \to -\infty$, we obtain $\overline{\overline{\phi}} = A(k,l,t)\mathrm{e}^{\rho z}$. Hence, (A 2)–(A 3) become

$$\epsilon \mathrm{i}kA + \epsilon A_t + \overline{\overline{\xi}} = 0, \qquad z = 0, \tag{A 5}$$

$$\rho A - \mathrm{i}k\overline{\overline{\xi}} - \overline{\overline{\xi}}_t = 0, \qquad z = 0. \tag{A 6}$$

Taking the Fourier transform of the initial condition on the free surface (A 4), using the appropriate integral identity from Gradshteyn & Ryzhik (1994), gives

$$\overline{\overline{\phi}}_0 = A(k,l,0) = -\frac{\mathrm{e}^{-\rho h}}{\rho}, \qquad \overline{\overline{\xi}}_0 = 0.$$

Using these initial conditions on A and $\overline{\overline{\xi}}$, we solve (A 5) and (A 6) and take the inverse Fourier transform to obtain

$$\hat{\xi} = \frac{1}{4\pi^2}\int_{-\infty}^{\infty}\int_{-\infty}^{\infty} \frac{\mathrm{i}\epsilon^{1/2}}{4\rho^{1/2}}\left[\mathrm{e}^{\mathrm{i}t\sqrt{\rho/\epsilon}} - \mathrm{e}^{-\mathrm{i}t\sqrt{\rho/\epsilon}}\right]\mathrm{e}^{-\rho h - \mathrm{i}kt}\mathrm{e}^{\mathrm{i}kx + \mathrm{i}ly}\,\mathrm{d}k\,\mathrm{d}l.$$

Setting (x,y) and (k,l) in terms of polar coordinates (r,θ) and (ρ,ϕ) respectively gives

$$\hat{\xi} = \int_0^{\infty}\int_0^{2\pi} \frac{\mathrm{i}\sqrt{\epsilon\rho}}{16\pi^2}\left[\mathrm{e}^{\mathrm{i}t\sqrt{\rho/\epsilon}} - \mathrm{e}^{-\mathrm{i}t\sqrt{\rho/\epsilon}}\right]\mathrm{e}^{-\rho h - \mathrm{i}t\rho\cos\phi}\mathrm{e}^{\mathrm{i}\rho r\cos(\theta-\phi)}\,\mathrm{d}\phi\,\mathrm{d}\rho.$$

Evaluating the inner integral gives

$$\hat{\xi} = \int_0^{\infty} \frac{\mathrm{i}\sqrt{\epsilon\rho}}{8\pi}\left[\mathrm{e}^{\mathrm{i}t\sqrt{\rho/\epsilon}} - \mathrm{e}^{-\mathrm{i}t\sqrt{\rho/\epsilon}}\right] J_0\left(\tfrac{1}{2}\rho\sqrt{t^2 + r^2 - 2tr\cos\theta}\right)\mathrm{e}^{-\rho h}\,\mathrm{d}\rho,$$

where J_0 is the Bessel function of the first kind. Approximating this integral using the method of stationary phase (valid when $t \gg \epsilon^{1/2}$) gives

$$\hat{\xi} \sim \frac{\epsilon^2}{\pi t^3}. \tag{A 7}$$

Consequently, we find that the free-surface behaviour contains a term which is singular at $t = 0$, and that only appears in terms that are $\mathcal{O}(\epsilon^2)$. This is the singularity that generates unsteady variation on the free surface. We emphasise that this is not a full representation of free-surface behaviour for the system under investigation in Section 2.2, but rather a single contribution to this behaviour that contains the singularity due to the sudden initial change.

Appendix B Numerical calculations

In order to verify the unsteady free-surface behaviour, we compare the position of the longitudinal wavefront to a numerical solution for the free-surface behaviour. We obtain

https://doi.org/10.1017/S0956792514000217 Published online by Cambridge University Press

this free-surface behaviour by formulating the solution to (2.1)–(2.6) in terms of a double integral which may be evaluated using standard numerical methods. Again, while we will formulate the double integral expression here, we note that similar integral expressions have been obtained in previous investigations, such as Havelock (1949).

To incorporate the behaviour of the source, we set

$$\phi = \frac{1}{4\pi\sqrt{x^2+y^2+(z-h)^2}} + \frac{1}{4\pi\sqrt{x^2+y^2+(z+h)^2}} + \hat{\phi}.$$

The linearized system (2.7)–(2.9) is given by

$$\nabla^2\hat{\phi} = 0, \qquad -\infty < z < 0, \tag{B 1}$$

$$\epsilon(\hat{\phi}_x + \hat{\phi}_t) + \xi = -\epsilon\left[\frac{1}{2\pi\sqrt{x^2+y^2+h^2}}\right]_x, \qquad z = 0, \tag{B 2}$$

$$\hat{\phi}_z - (\xi_x + \xi_t) = 0, \qquad z = 0. \tag{B 3}$$

Finally, the far-field conditions determine that $\hat{\phi} \to 0$ far from the source, and the initial condition is simply $\hat{\phi}_0 = 0$, $\hat{\xi}_0 = 0$. Taking the Fourier transform of (B 1) with respect to x and y (with the resultant expression given in terms of the Fourier variables k and l respectively) gives

$$\overline{\overline{\phi}}_{zz} - \rho^2\overline{\overline{\phi}} = 0,$$

where $\rho = \sqrt{k^2+l^2}$. Noting that the solution must decay in the limit that $z \to -\infty$, this differential equation may be solved to give $\overline{\overline{\phi}} = A(k,l,t)\mathrm{e}^{\rho z}$. Hence, (B 2) and (B 3) become

$$\epsilon \mathrm{i}kA + \epsilon A_t + \overline{\overline{\xi}} = -\frac{\mathrm{i}k\epsilon\mathrm{e}^{-\rho h}}{\rho},$$
$$\rho A - \mathrm{i}k\,\overline{\overline{\xi}} - \overline{\overline{\xi}}_t = 0,$$

where the appropriate integral expression from Gradshteyn & Ryzhik (1994) is used to compute the Fourier transform of the inhomogeneous term in (B 2). Applying the initial conditions and solving this system gives

$$\overline{\overline{\xi}} = \frac{\mathrm{i}k\epsilon\mathrm{e}^{-\rho h}}{2\rho(\rho-\epsilon k^2)}\left\{\left[(\rho + k\sqrt{\epsilon\rho})\mathrm{e}^{\mathrm{i}t\sqrt{p/\epsilon}} + (\rho - k\sqrt{\epsilon\rho})\mathrm{e}^{-\mathrm{i}t\sqrt{p/\epsilon}}\right]\mathrm{e}^{-\mathrm{i}kt} - 2\rho\right\}.$$

We formulate the inverse Fourier transform integral, representing (x,y) and (k,l) in terms of polar coordinates (r,θ) and (ρ,ϕ), giving

$$\overline{\overline{\xi}} = \frac{1}{4\pi^2}\int_0^{2\pi}\int_0^{\infty}\frac{\mathrm{i}\epsilon\rho\cos(\phi)\mathrm{e}^{-\rho h}}{2(1-\epsilon\rho\cos^2(\phi))}\left\{\left[(1+\cos(\phi)\sqrt{\epsilon\rho})\mathrm{e}^{\mathrm{i}t\sqrt{p/\epsilon}}\right.\right.$$
$$\left.\left. + (1-\cos(\phi)\sqrt{\epsilon\rho})\mathrm{e}^{-\mathrm{i}t\sqrt{p/\epsilon}}\right]\mathrm{e}^{-\mathrm{i}t\rho\cos(\phi)} - 2\rho\right\}\mathrm{e}^{\mathrm{i}\rho r\cos(\theta-\phi)}\,\mathrm{d}\rho\,\mathrm{d}\phi. \tag{B 4}$$

This integral is singular along the curve satisfying $1 - \epsilon\rho\cos^2(\phi) = 0$. To simplify the numerical evaluation of this double integral, we set the singular curve to follow a straight

https://doi.org/10.1017/S0956792514000217 Published online by Cambridge University Press

line. In this case, we apply the transformation $(u,v) = (\rho\cos^2(\phi), \phi)$, giving

$$\bar{\bar{\xi}} = \frac{1}{8\pi^2}\int_0^{2\pi}\int_0^{\infty} \frac{\mathrm{i}\epsilon u^2 \mathrm{e}^{-uh/\cos^2(v)}}{\cos^3(v)(1-\epsilon u)}\left\{\left[\left(1+\cos(v)\sqrt{\frac{\epsilon u}{\cos^2(v)}}\right)\mathrm{e}^{\mathrm{i}t\sqrt{u/\epsilon\cos^2(v)}}\right.\right.$$
$$\left.\left. + \left(1-\cos(v)\sqrt{\frac{\epsilon u}{\cos^2(v)}}\right)\mathrm{e}^{-\mathrm{i}t\sqrt{u/\epsilon\cos^2(v)}}\right]\mathrm{e}^{-\mathrm{i}tu/\cos(v)} - 2\right\}\mathrm{e}^{\mathrm{i}ur\cos(\theta-\phi)/\cos^2(v)}\,\mathrm{d}u\,\mathrm{d}v. \quad (B\,5)$$

This integral is substantially more complicated than the form given in (B 4). However, the fact that the integrand is singular along a straight line allows the double integral to be conveniently solved using standard numerical integration in two dimensions.

In order to evaluate (B 5) numerically for given values of h and ϵ, we again truncate the integral domain in the u-direction and split it into two regions, given by

$$D1 = \{(u,v) : u \in (0, 1/\epsilon - \Delta),\ v \in (0, 2\pi)\},$$
$$D2 = \{(u,v) : u \in (1/\epsilon + \Delta, u_\infty),\ v \in (0, 2\pi)\},$$

where Δ is a small constant used to approximate the Cauchy principal value integral, and u_∞ is the truncation point. Typical values used in this investigation are $\Delta = 1 \times 10^{-3}$ and $u_\infty = 50$. On each domain, we evaluate the two-dimensional integral numerically using the in-built MATLAB integrator, which uses two-dimensional quadrature techniques.

References

Abou-Dina, M. (2001) Nonlinear transient gravity waves due to an initial free-surface elevation over a topography. *J. Comp. App. Math.* **130**(1–2), 173–195.

Abramowitz, M. & Stegun, I. (1972) *Handbook of Mathematical Functions with Formulas, Graphs, and Mathematical Tables*, Dover Publications, New York.

Aoki, T., Koike, T. & Takei, Y. (2002) Vanishing of Stokes curves. In: T. Kawai & K. Fujita (editors), *Microlocal Analysis and Complex Fourier Analysis*, World Scientific, Singapore, pp. 1–22.

Chapman, S. J., King, J. R., Ockendon, J. R. & Adams, K. L. (1998) Exponential asymptotics and Stokes lines in nonlinear ordinary differential equations. *Proc. Roy. Soc. Lond.* A **454**(1978), 2733–2755.

Chapman, S. J. & Mortimer, D. B. (2005) Exponential asymptotics and Stokes lines in a partial differential equation. *Proc. Roy. Soc. Lond.* A **461**, 2385–2421.

Chapman, S. J. & Vanden-Broeck, J.-M. (2002) Exponential asymptotics and capillary waves. *SIAM J. Appl. Math.* **62**(6), 1872–1898.

Chapman, S. J. & Vanden-Broeck, J.-M. (2006) Exponential asymptotics and gravity waves. *J. Fluid Mech.* **567**, 299–326.

Cole, S. L. (1985) Transient waves produced by flow past a bump. *Wave Mot.* **7**, 579–587.

Craik, A. D. D. (2004) The origins of water wave theory. *Ann. Rev. Fluid Mech.* **36**(1), 1–28.

Dagan, G. & Tulin, M. P. (1972) Two-dimensional free-surface gravity flow past blunt bodies. *J. Fluid Mech.* **51**(3), 529–543.

Dingle, R. B. (1973) *Asymptotic Expansions: Their Derivation and Interpretation*, Academic Press, New York.

Forbes, L. K., Hocking, G. C. & Stokes, T. E. (2008) On starting conditions for a submerged sink in a fluid. *J. Eng. Math.* **61**, 55–68.

Gradshteyn, I. S. & Ryzhik, I. M. (1994) *Table of Integrals, Series, and Products*, Academic Press, New York.

https://doi.org/10.1017/S0956792514000217 Published online by Cambridge University Press

Grimshaw, R. (2011) Exponential asymptotics and generalized solitary waves. In H. Steinrück, F. Pfeiffer, F. G. Rammerstorfer, J. Salençon, B. Schrefler & P. Serafini (editors), *Asymptotic Methods in Fluid Mechanics: Survey and Recent Advances*, Vol. 523 of *CISM Courses and Lectures*, Springer, Vienna, pp. 71–120.

Grimshaw, R. & Joshi, N. (1995) Weakly nonlocal solitary waves in a singularly perturbed Korteweg-de Vries equation. *SIAM J. Appl. Math.* **55**(1), 124–135.

Havelock, T. H. (1917) Some cases of wave motion due to a submerged obstacle *Proc. Roy. Soc. Lond.* A **93**(654), 520–532.

Havelock, T. H. (1949) The wave resistance of a cylinder started from rest. *Quart. J. Mech. App. Math.* **2**(3), 325–334.

Howls, C. J., Langman, P. J. & Olde Daalhuis, A. B. (2004) On the higher-order Stokes phenomenon. *Proc. Roy. Soc. Lond.* A **460**(2121), 2285–2303.

John, F. (1953) Two-dimensional potential flows with a free boundary. *Comm. Pure Appl. Math.* **6**, 497–503.

Keller, J. B. & Ward, M. J. (1996) Asymptotics beyond all orders for a low Reynolds number flow. *J. Eng. Math.* **30**(1–2), 253–265.

Kelvin, B. W. T. (1887) On ship waves. *Proc. Inst. Mech. Eng.* **3**, 409–434.

Liu, M. & Tao, M. (2001) Transient ship waves on an incompressible fluid of infinite depth. *Phys. Fluids* **13**, 3610–3623.

Longuet-Higgins, M. S. (1980) A technique for time-dependent free-surface flows. *Proc. Roy. Soc. Lond.* A **371**, 441–451.

Lu, D. (2009) Generation of free-surface gravity waves by an unsteady Stokeslet. *Arch. App. Mech.* **79**, 311–322.

Lustri, C. J. & Chapman, S. J. (2013) Steady gravity waves due to a submerged source. *J. Fluid Mech.* **732**, 660–686.

Lustri, C. J., McCue, S. W. & Binder, B. J. (2012) Free surface flow past topography: A beyond-all-orders approach. *Euro. J. Appl. Math.* **23**(4), 441–467.

Lustri, C. J., McCue, S. W. & Chapman, S. J. (2013) Exponential asymptotics of free surface flow due to a line source. *IMA J. App. Math.* **78**(4), 697–713.

Ockendon, J. R., Howison, S., Lacey, A. & Movchan, A. (1999) *Applied Partial Differential Equations*, Oxford University Press, New York.

Ockendon, J. R. & Wilmott, P. (1986) Matching and singularity distributions in inviscid flow. *IMA J. App. Math.* **37**(3), 199–211.

Ogilvie, T. F. (1968) *Wave Resistance: The Low Speed Limit*, Technical report, Michigan University, Ann Arbor, MI.

Olde Daalhuis, A. B., Chapman, S. J., King, J. R., Ockendon, J. R. & Tew, R. H. (1995) Stokes phenomenon and matched asymptotic expansions. *SIAM J. App. Math.* **55**(6), 1469–1483.

Peregrine, D. H. (1972) A line source beneath a free surface, Mathematics Research Center Technical Summary Report 1248, University of Wisconsin, Madison, WI.

Shen, M. (1969) Asymptotic theory of unsteady three-dimensional waves in a channel of arbitrary cross section. *SIAM J. App. Math.* **17**(2), 260–271.

Stokes, G. G. (1864) On the discontinuity of arbitrary constants which appear in divergent developments. *Trans. Cam. Phil. Soc.* **10**, 105.

Stokes, T., Hocking, G. & Forbes, L. (2003) Unsteady free-surface flow induced by a line sink. *J. Eng. Math.* **47**, 137–160.

Trinh, P. H. (2011) Exponential asymptotics and Stokes line smoothing for generalized solitary waves. In: H. Steinrück, F. Pfeiffer, F. G. Rammerstorfer, J. Salençon, B. Schrefler & P. Serafini (editors), *Asymptotic Methods in Fluid Mechanics: Survey and Recent Advances*, Vol. 523 of *CISM Courses and Lectures*, Springer, Vienna, pp. 121–126.

Trinh, P. H. & Chapman, S. J. (2010) *Exponential Asymptotics and Free-surface Flows*, PhD Thesis, University of Oxford.

Trinh, P. H. & Chapman, S. J. (2013a) New gravity-capillary waves at low speeds. Part 1. Linear geometries. *J. Fluid Mech.* **724**, 367–391.

Trinh, P. H. & Chapman, S. J. (2013b) New gravity-capillary waves at low speeds. Part 2. Nonlinear geometries. *J. Fluid Mech.* **724**, 392–424.

Trinh, P. H., Chapman, S. J. & Vanden-Broeck, J.-M. (2011) Do waveless ships exist? Results for single-cornered hulls. *J. Fluid Mech.* **685**, 413–439.

Tyvand, P. A. (1992) Nonlinear transient freesurface flow and dip formation due to a point sink. *Phys. Fluids* A **4**, 671–676.

Tyvand, P. A. (1993) Unsteady free surface flow due to a line source. *Phys. Fluids* A **5**, 1368–1375.

Tyvand, P. A. & Miloh, T. (1995a) Free-surface flow due to impulsive motion of a submerged circular cylinder. *J. Fluid Mech.* **286**, 67–101.

Tyvand, P. A. & Miloh, T. (1995b) Free-surface flow generated by a small submerged circular cylinder starting from rest. *J. Fluid Mech.* **286**, 103–116.

Vanden-Broeck, J.-M., Schwartz, L. W. & Tuck, E. O. (1978) Divergent low-Froude number series expansion of non-linear free-surface flow problems. *Proc. Roy. Soc. Lond.* A **361**(1705), 207–224.

Wilmott, P. (1987) On the motion of a small two-dimensional body submerged beneath surface waves. *J. Fluid Mech.* **176**, 465–481.

Xue, M. & Yue, D. K. P. (1998) 'Nonlinear free-surface flow due to an impulsively started submerged point sink. *J. Fluid Mech.* **364**, 325–347.

Zhu, S. & Zhang, Y. (1997) On nonlinear transient free-surface flows over a bottom obstruction. *Phys. Fluids* **9**, 2598–2604.